Three-Dimensional Observation of Polymer Blend by X-ray Phase Tomography

Atsushi Momose*

Department of Advanced Materials Science, Graduate School of Frontier Sciences, The University of Tokyo, 5-1-5 Kashiwanoha, Kashiwa, Chiba 277-8561, Japan

Akiko Fujii†

Department of Applied Physics, The School of Engineering, The University of Tokyo, 5-1-5 Kashiwanoha, Kashiwa, Chiba 277-8561, Japan

Hidekazu Kadowaki and Hiroshi Jinnai

Department of Polymer Science and Engineering, Kyoto Institute of Technology, Matsugasaki, Sakyoku, Kyoto 606-8585, Japan

Received May 2, 2005

Introduction

Blending polymers is important because the properties of plastic materials can be tailored to meet various demands, which is not possible with a single polymer. Phase separation occurs in polymer blends and plays a significant role in determining their properties. Although phase-separated structures have been studied two-dimensionally for technical convenience, important quantities in three-dimensional space, such as the volume fractions of phases, the interfacial areas between coexisting phases, and interfacial curvatures, cannot be evaluated. It is clear that three-dimensional observation and analysis should be performed for the complete understanding of polymer blend morphologies.

The sizes of phase-separated structures range from nanometers to millimeters depending on the type of materials, and some techniques have been developed for the three-dimensional observation of phase-separated structures.[1] Laser scanning confocal microscopy has advanced the frontier of optical microscopy, enabling the three-dimensional observation of polymer blends[2−4] provided the sample is transparent in the region of interest. To reveal nanostructures three-dimensionally, transmission electron microtomography has also been developed and applied to block copolymer systems.[5,6] X-ray microtomography[7] and three-dimensional nuclear magnetic resonance imaging[8] are also used to observe opaque samples with a comparatively large field of view. All the three-dimensional observation methods mentioned above require chemical treatment for contrast enhancement, such as labeling or etching. However, it is preferable to observe a sample as is because chemical treatment may affect its properties. Moreover, when the growth of phase-separated structures is of interest, etching is not compatible with such measurement for tracing it in a sample.

We describe the potential superiority of X-ray phase tomography[9] to conventional X-ray microtomography. In general, X-ray image contrast is generated by a difference in X-ray absorption coefficient. For polymers, however, since the X-ray absorption coefficient is small and very weakly depends on the type of spices, the X-ray image contrast is poor. Therefore, a treatment for contrast enhancement is required. On the other hand, the X-ray phase shift induced by polymers is significantly large even if the X-ray attenuation is low. X-ray phase tomography measures such X-ray phase shift and reconstructs a tomogram that maps the refractive index difference, which is roughly proportional to the mass density of polymers. The high sensitivity of X-ray phase tomography has been demonstrated in the observation of biological tissues.[10−12] Since the density resolution of X-ray phase tomography is on the order of mg/cm^3, polymer blends should be within the scope of this method. In this study, we demonstrate the feasibility of X-ray phase tomography by observing three-dimensional phase-separated structures in a nontreated blend of polystyrene (PS) and poly(methyl methacrylate) (PMMA), which cannot be observed by any other techniques.

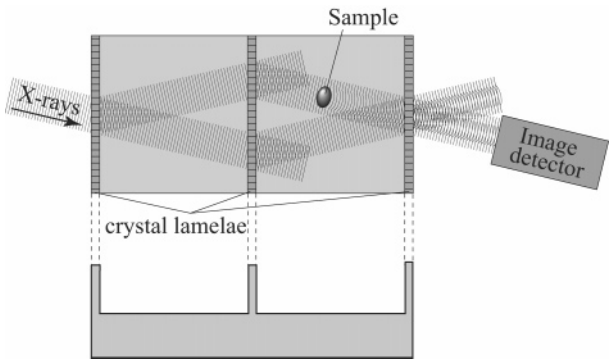

Figure 1. Crystal X-ray interferometer and beam paths.

X-ray Phase Tomography

In the X-ray energy region, the complex refractive index n is given by

$$n = 1 - \delta - i\beta \tag{1}$$

$$\delta = \frac{r_e \lambda^2}{2\pi} \rho \tag{2}$$

$$\beta = \frac{\lambda}{4\pi} \mu \tag{3}$$

where r_e, λ, ρ, and μ are the classical electron radius, X-ray wavelength, electron density, and linear absorption coefficient, respectively. δ and β are related to the X-ray phase shift and absorption, respectively. The ratio δ/β is about 10^3 for materials consisting of light elements, such as carbon. Therefore, an extremely high sensitivity is attained by detecting the X-ray phase shift compared with conventional X-ray imaging that relies on absorption.

The sensitivity of X-ray microtomography can be markedly improved by reconstructing an image from the

† Present address: Toshiba Corporation Semiconductor Company, Process & Manufacturing Engineering Center, 8 Shinsugita-Cho, Isogo-Ku, Yokohama 235-8522, Japan.

* Corresponding author: e-mail momose@exp.t.u-tokyo.ac.jp.

10.1021/ma050917o CCC: $30.25
Published on Web 07/09/2005

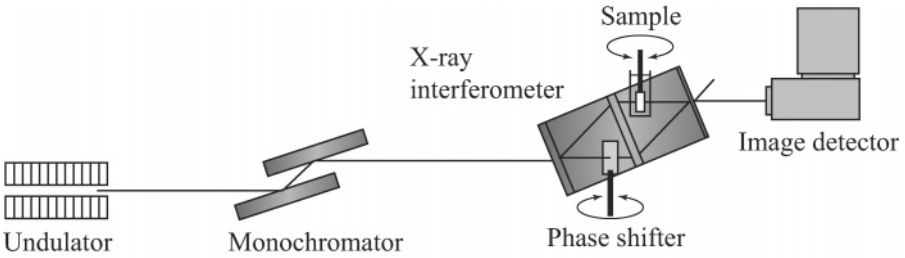

Figure 2. Experimental setup for phase tomography with crystal X-ray interferometer using synchrotron radiation.

X-ray phase shift as well. The X-ray phase shift Φ is given by

$$\Phi = \frac{2\pi}{\lambda}\int \delta \, dz \tag{4}$$

where z is the beam propagation direction. Because Φ is a projection of δ, δ can be reconstructed in a tomographic configuration if the phase shift is measured in plural projection directions. Such reconstruction is called X-ray phase tomography.

The X-ray phase shift can be measured using a crystal X-ray interferometer.[13] As shown in Figure 1, the interferometer has three crystal lamellae, cut out monolithically from a silicon crystal block with the same spacing. When an X-ray beam satisfies the Bragg diffraction condition against the lattice planes perpendicular to the surface of the first lamella, the X-ray beam is divided coherently into two beams going out of the opposite surface of the lamella. The two beams are diffracted at the second lamella in the same manner, and two beams converging onto the third lamella are also diffracted, thereby producing interfering beams. When a sample is placed in one of the paths, the interference pattern $I(x,y)$, which is generally given by

$$I(x,y) = a(x,y) + b(x,y)\cos\{\Phi(x,y) + \Delta(x,y)\} \tag{5}$$

is observed.[11] Here, $a(x,y)$ and $b(x,y)$ are the average intensity and fringe contrast, respectively. $\Delta(x,y)$ denotes the built-in pattern due to imperfections in the interferometer. x and y are the coordinates of the image.

$\Phi(x,y)$ can be measured by a fringe-scanning technique. When the phase differences $2\pi k/M$ between the two arms are introduced by a tunable phase shifter

$$I_k(x,y) = a(x,y) + b(x,y)\cos\left\{\Phi(x,y) + \Delta(x,y) + \frac{2\pi k}{M}\right\} \quad (k = 1, 2, ..., M) \tag{6}$$

are observed, where M is an integer. Then, $\Phi(x,y)$ is obtained from

$$\Phi(x,y) + \Delta(x,y) = \arg\left[\sum_{k=1}^{M} I_k(x,y)\exp\left(-2\pi i\frac{k}{M}\right)\right] \tag{7}$$

where arg[ ] denotes the extraction of the argument.[14] $\Delta(x,y)$ can be determined in the same manner without a sample ($\Phi(x,y) = 0$). By repeating this measurement at every angular step of sample rotation, a data set for tomographic reconstruction is collected.

Experimental Section

Samples. A PS/PMMA blend is immiscible and readily forms phase-separated structures; thus, we selected it as a model sample in this study. The densities of PS and PMMA are 1.04−1.06 and 1.18−1.20 g/cm^3, respectively. Because the difference in density between the two components exceeds the density resolution of X-ray phase tomography, which was 4 mg/cm^3 in a previous biological imaging result,[10] a clear contrast distinguishing PS from PMMA is expected in the phase tomograms. The weight-average molecular weight (M_w) and polydispersity index (M_w/M_n) of PS were 76 500 and 1.04, respectively. The M_w and M_w/M_n of PMMA were 33 200 and 1.08, respectively. A benzene solution containing 50 vol % PS and 50 vol % PMMA was freeze-dried. The resulting freeze-dried powder was annealed at 180 °C for 3 h, which was considered to be the phase separation time, in cylindrical holes (2 mm in diameter) made on a copper plate sandwiched in a melt-press machine.

Experimental Setup. X-ray phase tomography was performed using synchrotron radiation at the beamline 20XU of SPring-8, Japan. Figure 2 shows the experimental setup. X-rays from an undulator were monochromatized at 17.7 keV by a Si 111 double-crystal monochromator and introduced into an X-ray interferometer. The third lamella of the interferometer was thinned down to 40 μm to avoid image blurring.[12] A blend sample was fixed on a rotation rod and put in a cell filled with water, which was placed in the X-ray beam path of the interferometer. For the tomographic scan, the rod with the sample was rotated in the cell. The water-filled cell was necessary so that the difference in refractive index between the sample and its surrounding medium was moderately small. If the sample was observed in air, the fringe spacing became too narrow to resolve. A phase shifter (glass plate, 0.3 mm in thickness) was placed on the other beam path to perform fringe scan; by rotating the plate, its effective thickness was controlled, thereby inducing tuned X-ray phase shift. Interference patterns were recorded using a CCD-based image detector (Hamamatsu Photonics K.K., C4742-98) with a 10 μm thick luminescent screen (Gd_2S_2O:Tb) and a lens coupling. The effective pixel size was 3.14 μm.

Scan Parameters of Phase Tomography. The sample was rotated in 0.45° steps, and 400 maps of X-ray phase shift Φ were measured. Each X-ray phase shift map was obtained using eq 7 by four-step fringe scan ($M = 4$).

Results and Discussion

Figure 3 shows a tomogram and a three-dimensional rendering view of the reconstructed data of the PS/PMMA blend. Two phases in the blend were clearly depicted, and bicontinuous phase-separated structures were revealed. The volume ratio of the two phases was evaluated to be 52:48, in agreement with the blend composition. The spatial resolution of the phase tomogram was evaluated to be 10 μm from the contrast profile between the sample and the surrounding water.

The image maps the difference in δ between the sample and water, and bright and dark areas in Figure 3a correspond to PMMA- and PS-rich phases, which were confirmed from the histogram of the reconstructed values shown in Figure 4. The arrows indicate the values 1.21×10^{-8} and 1.15×10^{-7}, which were calculated for pure PS and PMMA under the assumption that the densities of PS and PMMA were 1.05 and 1.19 mg/cm^3, respectively. The peaks of the histogram

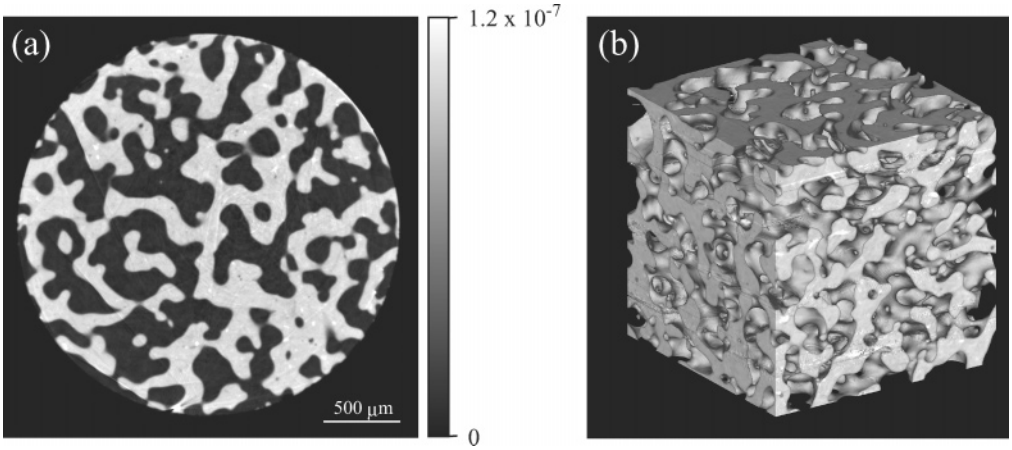

Figure 3. Reconstructed image of PS/PMMA blend by X-ray phase tomography: (a) phase tomogram and (b) volume rendering view of reconstructed three-dimensional data, where PS region has been made transparent.

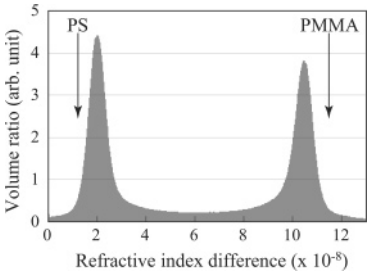

Figure 4. Histogram of refractive index difference between sample and water. The refractive index differences of pure PS and PMMA estimated from the densities are indicated by arrows.

appeared slightly inside the arrows, indicating that the PS-rich phase contained a small amount of PMMA and vice versa. This result quantitatively suggests that X-ray phase tomography can be used not only to depict structures but also to measure the composition of each phase, thereby allowing the determination of a phase diagram.

The detection limit of the density deviation of X-ray phase tomography under the present conditions was evaluated from the standard deviation of the reconstructed values of the tomogram. The standard deviation in the water region, which is outside the sample, was 8.7×10^{-10}. Because the δ of water is 7.4×10^{-7} for the 17.7 keV X-rays used in the present measurement, the density resolution was estimated to be 3.6 mg/cm^3 (3-fold the standard deviation).

Some artifacts, however, appeared because of the error in resolving fine fringes in the phase measurement. The fringe spacing is enlarged using X-rays of higher energy since X-ray phase shift is proportional to X-ray wavelength. The error can therefore be avoided to some extent by selecting a suitable X-ray energy depending on the type of sample.

X-ray phase tomography is thus demonstrated to be an attractive technique for the three-dimensional observation of a polymer blend as is. Since no treatment is required for contrast enhancement, some intriguing experiments, such as the in situ three-dimensional tracing of phase separation and the observation of structural changes under mechanical stress, would be feasible. In addition, X-ray phase tomography can contribute to the observation of not only binary blends but also ternary[15] and more complex blends.

Conclusions

We have applied X-ray phase tomography to the quantitative three-dimensional observation of phase-separated structures of a PS/PMMA blend without treatment for contrast enhancement. We observed a clear contrast between PS- and PMMA-rich phases at a spatial resolution of 10 μm. The contrast resolution, in terms of density resolution, was 3.6 mg/cm^3. The image quality attained by X-ray phase tomography is thus excellent for the three-dimensional evaluation of polymer blends, providing various research opportunities that are not possible by other methods. In combination with sophisticated techniques of three-dimensional image analysis, X-ray phase tomography is attractive for the unique structural studies of polymer blends.

Acknowledgment. Authors are grateful for the technical support by Drs. Yoshio Suzuki and Kentaro Uesugi in the experiment using synchrotron radiation, which was performed under the approval of SPring-8 committee 2004B0706-NM-np. A.F. was supported in the experiment by SPring-8 Budding Researchers Support. H.J. is grateful to the New Energy and Industrial Technology Development Organization (NEDO) for supporting this study through a Project on "Nano Structured Polymeric Materials".

References and Notes

(1) Jinnai, H.; Ikehara, T.; Nishi, T. *Adv. Polym. Sci.* **2004**, *170*, 115.
(2) Verhoogt, H.; Van Dam, J.; Posthuma de Boer, A.; Draaijer, A.; Houpt, P. M. *Polymer* **1993**, *34*, 1325.
(3) Jinnai, H.; Koga, T.; Nishikawa, Y.; Hashimoto, T.; Hyde, S. T. *Phys. Rev. Lett.* **1997**, *78*, 2248.
(4) Jinnai, H.; Nishikawa, Y.; Morimoto, H.; Koga, T.; Hashimoto, T. *Langmuir* **2000**, *16*, 4380.
(5) Spontak, R. J.; Fung, K. C.; Braunfeld, M. B.; Sedat, J. W.; Agard, D. A.; Kane, L.; Smith, S. D.; Satkowski, M. M.; Ashraf, A.; Hajduk, D. A.; Gruner, S. M. *Macromolecules* **1996**, *29*, 4494.
(6) Jinnnai, H.; Nishikawa, Y.; Spontak, R. J.; Smith, S. D.; Agard, D. A.; Hashimoto, T. *Phys. Rev. Lett.* **2000**, *84*, 518.
(7) Mashita, N.; Minamikawa, T.; Uesugi, K.; Jinnai, H. *Kobunshi Ronbunshu* **2003**, *60*, 373.
(8) Koizumi, S.; Yamane, Y.; Kuroki, S.; Ando, I.; Nishikawa, Y.; Jinnnai, H., manuscript in preparation.
(9) Momose, A. *Nucl. Instrum. Methods A* **1995**, *352*, 622.
(10) Momose, A.; Takeda, T.; Itai, Y.; Hirano, K. *Nature Med.* **1996**, *2*, 473.
(11) Momose, A.; Hirano, K. *Jpn. J. Appl. Phys.* **1999**, *Suppl. 38−1*, 625.

(12) Momose, A.; Koyama, I.; Hamaishi, Y.; Yoshikawa, H.; Takeda, T.; Wu, J.; Itai, Y.; Takai, K.; Uesugi, K.; Suzuki, Y. *J. Phys. IV* **2003**, *104*, 599.
(13) Bonse, U.; Hart, M. *Appl. Phys. Lett.* **1965**, *6*, 155.
(14) Bruning, J. H.; Herriott, D. R.; Gallagher, J. E.; Rosenfield, D. P.; White, A. D.; Brangaccio, D. J. *Appl. Opt.* **1974**, *13*, 2693.
(15) Nauman, E. B.; He, D. Q. *Polymer* **1994**, *35*, 2243.

MA050917O